Final report for DOE award DE-FG02-07ER46400, Northeastern University
360 Huntington Avenue, Boston, Massachusetts, 02115

Project title and PI: Phase-Field Modeling of Materials Interfaces and Nanostructures, Alain Karma, PI (a.karma@northeastern.edu)

Period: 7/15/2007-/7/14/2022

Project goals

Nanostructured materials offer unique properties for a wide range of energy applications. Among various known processing methods, liquid metal dealloying (LMD)—the selective dissolution of a base alloy element into a metallic melt—has emerged as a powerful technique to produce a new class of nano-/meso-scale open porous and bicontinuous composite structures with ultra-high interfacial area. LMD has recently been complemented by the advent of vapor phase dealloying (VPD), a novel technique that exploits the selective evaporation of one element from a parent alloy containing elements with very different vapor pressures, thereby enabling to fabricate open nanoporous structures of various elements from less-noble metals to inorganic elements regardless of their chemical activity without requiring high LMD temperatures and chemical etching. Together LMD and VPD have greatly expanded the scope of dealloying techniques, limited by traditional electrochemical means to noble metals, and boosted the design of new functional and structural materials that combine a wide variety of elements. Topologically-connected open porous structures with ultra-high surface area allow mass transport within the structure while preserving structural integrity, enabling them to serve as catalysts, fuel cells, supercapacitors, or high-capacity battery materials. Bicontinuous composite structures in turn can display high strength and high ductility or superior radiation-damage resistance due to the ultra-high interface area between interpenetrating solid phases. This research program makes use of state-of-the-art computational methods to understand at a basic level the self-organizing dealloying process with main focus on dealloying kinetics and interfacial pattern formation at the dealloying front controlling initial structure size, topology, and phase compositions. Phase-field simulation studies of LMD focus on solid solutions, line compounds, and intermetallic systems that can form ternary composites by nucleation and growth of a new phase. Studies of VPD employ phase-field modeling and a hybrid method combining a kinetic Monte Carlo (KMC) model of evaporation and surface diffusion with molecular dynamics for vapor-phase transport inside nanopores. Simulations explore mechanisms of interface- and diffusion-controlled dealloying kinetics, both observed in VPD but not fundamentally understood. In addition, our newly developed multi-physics phase-field approach of large-volume-change phase transformations is being used to model novel 3D anode geometries based on dealloyed nanoporous structures including novel sandwiched graphene/Si/silica for high-rate Li ion battery. Those studies are aimed at elucidating geometric design principles that improve mechanical stability. We expect this research to enhance the capability to tailor nano-/mesoscale structures for a wide range of energy-related materials applications and to yield further advances in computational methodologies that benefit a broad materials research community.

Grain-boundary premelting and shearing. We have performed a detailed study of grain-boundary premelting using the phase-field crystal (PFC) model. Our results demonstrate that there is a qualitative difference between high-angle repulsive and low-angle attractive grain boundaries. In the former, a continuous liquid film forms below the melting point, exhibiting a width that diverges when the melting point is approached from below. For low-angle grain boundaries, melting starts at individual dislocations. The grain boundary can be overheated up to a misorientation- dependent critical temperature at which the solid bridges be- tween the liquid pools break and the system becomes liquid. Furthermore, we have found that a hysteretic structural transition from single dislocations to dislocation pairs can occur for intermediate values of the misorientation. We have also used the PFC method to investigate the equilibrium premelting and nonequilibrium shearing behaviors of [001] symmetric tilt grain boundaries (GBs) at high homologous temperature in classical models of bcc Fe, and also compared our equilibrium results to MD simulations.

Dislocation-pairing transitions in hot grain boundaries. We have discovered a novel grain-boundary structural phase transition in both molecular-dynamics and phase-field-crystal simulations of classical models of bcc Fe. This transition is characterized by pairing of individual dislocations with mixed screw and edge components. We have demonstrated that this type of transition is driven by a combination of factors including elastic softening, core interaction, and core disordering. At high homologous temperatures the occurrence of this transition is shown to prevent premelting at misorientation angles where it would otherwise be expected.

Theory of polycrystalline pattern evolution. The rate of curvature-driven grain growth in polycrystalline materials is known to be limited by interface dissipation. We have shown analytically and by phase-field-crystal simulations that, for systems forming modulated phases or nonequilibrium patterns with crystal ordering, growth is limited by bulk dissipation associated with lattice translation, which dramatically slows down grain coarsening. We have also shown that bulk dissipation is reduced by thermal noise and that this reduction leads to faster coarsening behavior dominated by interface dissipation for a high Peierls-Nabarro barrier to dislocation motion and high noise. Those results provide a unified theoretical framework for understanding and modeling polycrystalline pattern evolution in diverse systems over a broad range of length and time scales.

Surface modes of spinodal decomposition. We have used linear stability theory and numerical simulations to show that spontaneous phase separation in elastically coherent solids is fundamentally altered by the presence of free surfaces. Because of misfit stress relaxation near surfaces, phase separation is mediated by unique surface modes of spinodal decomposition that have faster kinetics than bulk modes and are unstable even when spinodal decom- position is suppressed in the bulk. Consequently, in the presence of free surfaces, the limit of metastability of supersaturated solid solutions of crystalline materials is shifted from the coherent to chemical spinodal. The results provide guidance for controlling surface modes of coherent spinodal decomposition to produce desired nanostructures.

Morphological instability of grain boundaries in two-phase coherent solids. We have shown both computationally and analytically that grain boundaries (GBs) that exhibit shear-coupled motion become morphologically unstable in solid alloys that phase separate into coherent domains

of distinct chemical compositions. We carried out simulations of continuum models demonstrating that this instability is mediated by long-range elastic interaction between compositional domains and grain boundaries. In addition, we performed a linear stability analysis that predicts the range of unstable wavelengths in good quantitative agreement with simulations. In nonlinear stages, this pattern-forming instability leads to the breakup of low-angle grain boundaries, thereby strongly impacting microstructural evolution in a wide range of phase-separating materials. The results provide a theoretical basis for understanding the complex interaction between GBs and precipitates formed by nucleation or spinodal decomposition in a wide range of two-phase materials.

Relationship between equilibrium fluctuations and shear-coupled motion of grain Boundaries. We derived general analytical expressions relating the equilibrium fluctuations of a grain boundary to key parameters governing its motion coupled to shear deformation. We validated these expressions by molecular dynamics simulations for symmetrical tilt boundaries and demonstrate how they can be used to extract the misorientation dependence of the grain-boundary mobility. The results shed light on fundamental relationships between equilibrium and nonequilibrium grain-boundary properties and provide new means to predict those properties.

Topology-generating interfacial pattern formation during liquid metal dealloying. Liquid metal dealloying has emerged as a novel technique to produce topologically complex nanoporous and nanocomposite structures with ultra-high interfacial area and other unique properties relevant for diverse material applications. This process is empirically known to require the selective dissolution of one element of a multicomponent solid alloy into a liquid metal to obtain desirable structures. However, how structures form is not known. We have demonstrated, using mesoscale phase-field modelling and experiments, that nano/microstructural pattern formation during dealloying results from the interplay of interfacial spinodal decomposition, forming compositional domain structures enriched in the immiscible element, and diffusion-coupled growth of the enriched solid phase and the liquid phase into the alloy. We have further shown that those two mechanisms interact to yield a rich variety of topologically disconnected and connected structures and derived scaling laws governing microstructural length scales and dealloying kinetics.

Vapor-phase dealloying. Vapor phase dealloying (VPD) is an environmentally-friendly method for fabricating nanoporous materials by utilizing the saturated vapor pressure difference of elements to selectively drive sublimation of one or more components from an alloy. VPD kinetics has not been explored and rate-controlling factors of the solid-gas transformation within complex nanostructure remain unknown. Using manganese-zinc alloys as a prototype system, we systematically investigated the dependence of dealloying velocity on temperature and pressure and presented a model to quantitatively describe the dealloying kinetics. We found that the dealloying velocity exhibits a linear to power law transition at a critical dealloying depth, resulting from the interplay between the kinetic process of dealloying and dealloyed microstructure. This transition bridges ballistic evaporation at early time to Knudsen diffusion of Zn vapor in developed pore channels where the Zn partial pressure at the dealloying front reaches the local equilibrium between the solid and vapor phases. By comparing activation energies for VPD and bulk zinc sublimation, the entire energy landscape of VPD is measured. The fundamental understanding of VPD kinetics paves an effective way to design dealloyable precursor alloys and to optimize dealloyed microstructure of VPD materials for a wide range of applications.

Nano-/meso-scale bicontinuous structures formation by peritectic melting. To produce topologically connected bicontinuous structures, LMD has traditionally required minimally a ternary system consisting of the two elements of the base alloy and a different third element of the liquid melt chosen so as to selectively dissolve one of the elements of the base alloy, as exemplified by dealloying of TaTi alloys by a Cu melt, which has served as model system for fundamental experimental studies of LMD structures and kinetics. However, a recent experimental study has shown that bicontinuous structures similar to those produced by LMD can be obtained by isothermal melting of a peritectic TiAg binary alloy. Those observations raise the interesting question of whether the "topology-generating" interfacial pattern formation mechanism in a binary system differs fundamentally from the one previously elucidated for LMD in ternary systems. In the latter, pattern formation involved both interfacial spinodal decomposition to form Ta-rich regions along the solid-liquid interface and two-phase coupled growth to propagate liquid channels inside the base alloy. They also raise the broader question of which of those mechanisms underlies structure formation in more complex alloy systems forming intermetallic compounds (e.g. dealloying of SiC by a Ge melt through the reaction SiC → Si + C), which bear similarity to peritectic systems. To investigate the first question above, we used 2D and 3D simulations of a multiphase-field model of Lo et al. previously developed in the PI's group with model parameters adapted to model isothermal melting of a peritectic TiAg alloy. Melting decomposes the solid β phase of the base alloy of peritectic composition into a Ti-rich solid α phase and a Ag-rich liquid phase. Our 2D and 3D simulations results (Fig. 1) reveal striking similarities but also important differences between pattern formation in LMD and peritectic melting. During LMD in ternary systems (solid solution dealloyed by a liquid melt), the formation of the solid phase that is rich in the non-dissolving element has been shown to be controlled by interfacial spinodal decomposition, which is absent in peritectic melting. In the latter, formation of the analogous α phase is controlled by nucleation at the solid-liquid interface (Fig. 1A showing structures with nucleation rate of α at the β −liquid interface decreasing from left to right with liquid: red, blue: α, light blue: β). At a high nucleation rate, repeated heterogeneous nucleation events at the solid-liquid interface alters the growth direction of liquid channels forcing

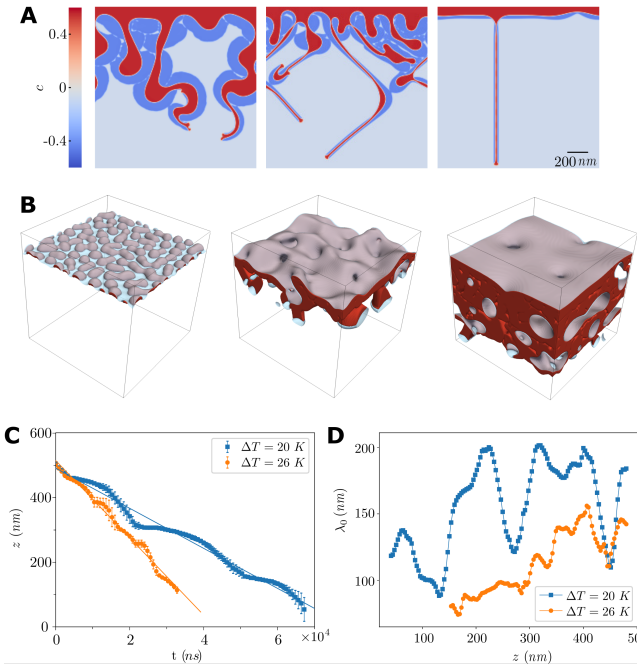

Fig. 1. Phase-field simulations of isothermal melting of a peritectic TiAg alloy showing the formation of bicontinuous composite structures. (**A**) Decreasing the nucleation rate in 2D simulations significantly affects the morphology. Snapshots of 3D simulations at successive times (**B**) showing that the growth of the dealloying front has a constant velocity (**C**), which can be increased by increasing the processing temperature. (**D**) Depenence of the ligament size on temperature. The 2D and 3D simulation sizes are 1638 nm × 1638 nm and 614 nm × 614 nm × 610 nm, respectively.

them follow tortuous paths and gives rise to polycrystalline structures with a grain size comparable to the ligament size. In contrast, at low nucleation rate, re-nucleation is absent, thereby alloying liquid channels to grow straight into the base alloy. In 3D simulations (Fig. 1B), porous structure formation occurs consistent with experimental observations. In Fig. 1B, red indicates α phase, brown the liquid-α interface, and light blue the β −liquid interface with the liquid and the β phase at the top and bottom, respectively. To characterize the dealloying kinetics, we measured the dealloying front position as a function of time. The result shows that the dealloying depth increases linearly in time (Fig. 1C), in contrast to LMD where the depth increases $\sim t^{1/2}$. This difference stems from the fact that peritectic melting does not involve the long-range diffusive transport of the dissolving element from the dealloying front to the edge of the dealloyed layer that is responsible for the $t^{1/2}$ behavior. However, like in LMD, dealloying involves the diffusive coupled growth of liquid channels and the nearby solid α phase that controls the velocity of the front associated with lamellar growth in 2D (Fig. 1A) and worm-like growth in 3D (Fig. 2A). To study the effect of thermodynamic driving force, we carried out 3D simulations at higher superheating $\Delta T = T - T_p$, where T is the isothermal processing temperature and T_p is the peritectic temperature. The results show that the dealloying velocity increases with ΔT (Fig. 1C), accompanied by a decrease of average ligament size (Fig. 1D). To gain further insight into the pattern formation process, we investigated the growth properties of individual liquid channels. The results show that, in both 2D and 3D, the channel width decreases as $\sim \Delta T^{-2}$ (Fig. 2B) and the growth velocity is inversely proportional to this width (Fig. 2C). The channel width at $\Delta T = 20\ K$ and $\Delta T = 26\ K$ are comparable to the ligament sizes in Fig. 1D, supporting the interpretation that worm-like growth of individual liquid channels is the dominant mechanism controlling the growth kinetics and ligament size of bicontinuous composite structures (Fig. 1B). Repeated nucleation events deflect the trajectories of liquid channels, promoting the formation of topologically connected structures in 3D, but do not significantly alter their growth velocity and width. In addition, we found that the growth velocity scales proportionally to the liquid diffusivity (green triangles in Fig. 2C), further supporting the theoretical expectation that coupled growth is diffusion-controlled.

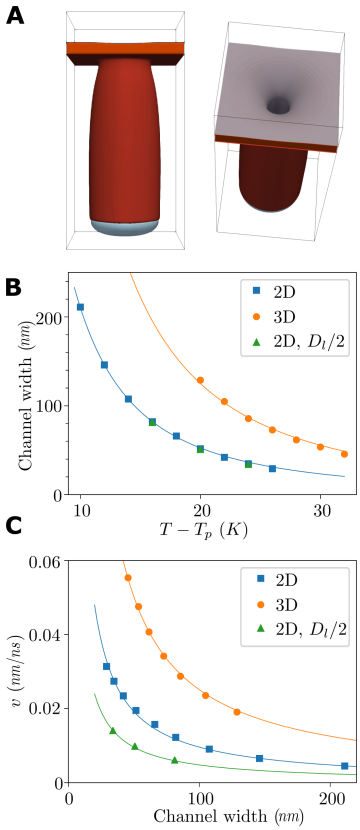

Fig. 2. Growth properties of individual liquid channels. (**A**) Example of worm-like morphology. (**B**) Channel width versus superheating $\Delta T = T - T_p$. (**C**) Growth velocity versus channel width.

Large-volume-change transformations in lithium-ion battery materials. With approximately ten times greater charge capacity over conventional carbon-based anodes, silicon and germanium have emerged as attractive anode materials for lithium-ion batteries. The improved charge capacity is accompanied by nearly 300% volume change during lithiation, which can lead to mechanical failure — notably fracture — and prevent these materials from seeing their full potential. Hence, research into Si- or Ge-based anodes has predominantly focused on shape design, for example hollow tubes and nanoporous architectures fabricated via liquid metal dealloying. To explore the

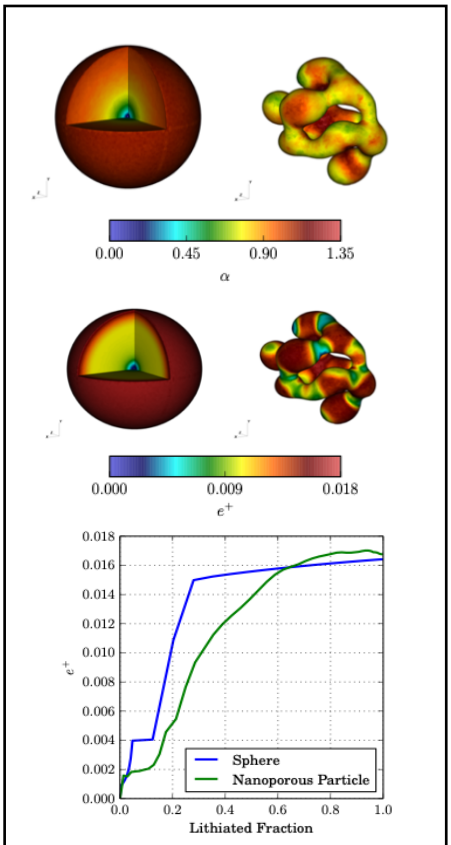

Fig. 3: Equivalent plastic strain (α, top) and non-compressive elastic energy density (e^+, middle) in a fully-lithiated sphere and nanoporous particle. The sphere has been cut away to show the distribution through the cross section. (Bottom) Maximum energy density versus fraction of the anode which has been lithiated.

role of anode shape on mechanical behavior, we have developed a model which couples phase-transition kinetics with volumetric swelling and elastoplastic material deformation at large strains. This model was previously applied to study lithiation of two-dimensional circular and annular domains (which represent the cross sections of cylinders and tubes, respectively). In these domains, it was shown that plastic localization caused the formation of V-shaped notches along the outer edge of the domain, which served as initiation points for potential fracture. In 3D, we studied how equivalent plastic strain α and the non-compressive elastic energy e^+ are affected by the topology during isotropic lithiation. The latter is important in understanding where cracks may nucleate in the specimen; in phase-field models, cracks nucleate when e^+ exceeds a critical threshold. Our first example was the comparison between a spherical particle and a nanoporous particle. The latter geometry was computed via simulation of liquid metal dealloying process and had approximately 50% porosity. We show the results for the two geometries in Fig. 3. The distribution of plastic strain and energy density was symmetric in the spherical particle. Meanwhile, the nanoporous particle experienced preferential accumulation of plastic strains in areas with negative surface curvature; V-shaped notches were absent. The same areas with plastic strain concentrations also experienced the highest energy densities; notably, these areas do not lie along the ligaments of the nanoporous geometry. Remarkably, the maximum energy density was comparable between the two geometries. The nanoporous geometry may be viewed as a collection of spheres connected by ligaments. To better understand the behavior of the ligaments, we considered two model geometries: the infinite cylinder and the torus. The nanoporous ligaments do not have uniform thickness; for the cylinder and torus, we also studied variations in the radii. The uniform cylinder (despite isotropic invasion) and torus experienced plastic strain concentrations along their length (in the case of the torus, along the inner wall), which can lead to V-shaped notches. Meanwhile, the non-uniform cylinder and torus did not see this behavior. Notably, the energy density pattern in the non-uniform torus resembled that in the nanoporous geometry. Based on the results for the cylinder and torus, the variable thickness of the ligaments in the nanoporous particle appear to prevent strong plastic localization (notably, V-shaped notches) along their lengths. Thus, the thick portions of the particle, which behave like spheres, experience the highest energy densities. However, in the nanoporous particle, the effective radii of the spheres are smaller, which make them more resistant to fracture than a single, larger spherical particle with equivalent volume.

Topological control of LMD structures. The past few years have witnessed the rapid development of LMD to fabricate nano-/meso-scale porous and composite structures with ultra-high interfacial area for diverse materials applications. However, this method currently has two important limitations. First, it produces bicontinuous structures with high-genus topologies for a limited range of alloy compositions. Second, structures have a large ligament size due to substantial coarsening during dealloying at high temperature. We have demonstrated computationally and experimentally that those limitations can be overcome by adding to the metallic melt an element that promotes high-genus topologies by limiting the leakage of the immiscible element during dealloying. We further interpreted this finding by showing that bulk diffusive transport of the immiscible element in the liquid melt strongly influences the evolution of the solid fraction and topology of the structure during dealloying. The results shed light on fundamental differences in liquid metal and electrochemical dealloying and establish a new approach to produce LMD structures with desired size and topologies.

Fragmentation of faceted nanowires. The reduction of surface energy is a well-known driving force for the fragmentation of nanowires. Fragmentation can limit the service life of those small low-dimensional building blocks or can be controlled to induce beneficial shape changes. For isotropic surface energy, fragmentation is analogous to the classic Rayleigh-Plateau instability of liquid jets. However, commonly synthesized crystalline nanowires have strongly anisotropic surface energies and exhibit facets coinciding with cusps in the Wulff plot. Depending on growth orientation, different fragmentation behaviors have been seen in nanowires. Using phase-field simulations, we have shown that fragmentation of faceted nanowires with cubic crystal symmetry may occur by a finite-amplitude nonlinear instability, as opposed to a Rayleigh-Plateau-like linear instability, depending on nanowire growth orientation. We carried out a weakly nonlinear analysis based on sharp interface theory to characterize the faceted nanowire shape corresponding to a surface-energy saddle point. The analysis predicts that the minimum amplitude of a periodic shape perturbation to trigger fragmentation increases with cusp strength but decreases inversely proportionally to the perturbation wavelength for long wavelengths, in good quantitative agreement with phase-field predictions. The results provide the theoretical foundation to predict nanowire stability as a function of length and surface energy in diverse applications.

Topology-enhanced mechanical stability of swelling nanoporous electrodes. Materials like silicon and germanium offer a 10-fold improvement in charge capacity over conventional graphite anodes in lithium-ion batteries but are subject to a roughly three fold increase in volume during lithiation, which presents a major challenge in ensuring battery integrity. Nanoporous silicon, created by LMD, has emerged as a potentially attractive anode design to cope with this challenge, exhibiting both higher capacity and extended cycle lifetimes. However, how nanoporous structures accommodate such a large volume change is unknown. We have addressed this question by using phase-field modeling to both produce low- and high-genus nanoporous particles and to investigate their elastoplastic swelling behavior and fracture (Fig. 4). Our results show that enhanced mechanical stability results from the unique network topology of nanoporous anodes consisting of ligaments connected by bulbous, sphere-like nodes. The ligaments forcefully resist elongation

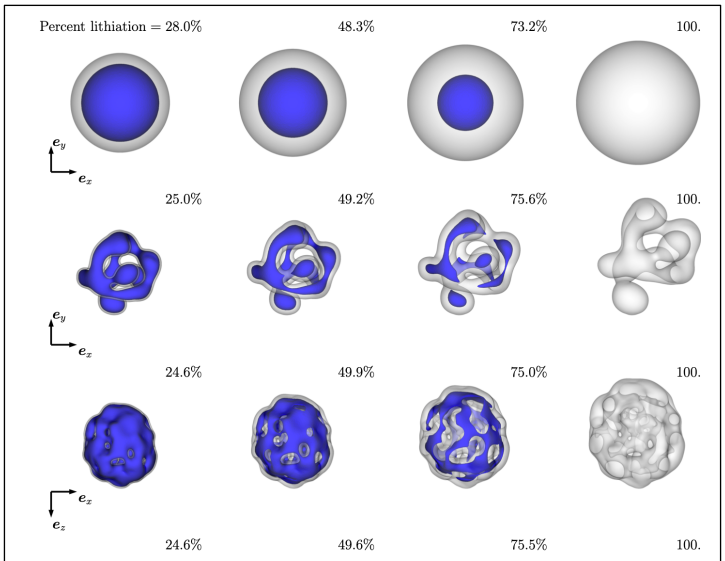

Fig. 4 Phase-field simulations of lithiation of spherical (top row) and swelling nanoporous electrodes (middle and bottom rows).

while the bulbous nodes, behaving similarly to isolated spherical particles, experience large stresses driving fracture. However, due to their much smaller size compared to a sphere of the same volume as the entire nanoporous particle, bulbous nodes in the network are more protected against fracture; this size effect results from both the standard assumed linear scaling of flaw size with particle size and the presence of stress gradients inherent in the lithiation process. In addition, even though nanoporous particles have ultra-high surface area compared with a sphere of identical volume, they have less overall surface area prone to damage.

Kinetic Monte Carlo study of vapor phase dealloying. Vapor phase dealloying (VPD) is a novel method that exploits the selective evaporation of one element of a solid binary alloy to synthesize high-genus open nanoporous structures of the other element with ultrahigh interfacial area for diverse applications. In a recent study summarized above, we have developed a simple analytical theory of VPD kinetics, which assumes that the dealloying rate is limited by Knudsen diffusion of evaporated atoms inside the dealloyed layer. To further test this theory, we have developed a lattice Kinetic Monte Carlo (KMC) model of VPD that incorporates surface diffusion and vapor phase transport inside the dealloyed layer in the physically relevant limit where the mean free path of evaporated atoms is much larger than the ligament size. In this limit, atoms simply undergo ballistic motion inside the open nanoporous structure. Importantly, atoms are allowed to stick again to the surface at the end of their ballistic trajectory, and not only reflect as assumed in Knudsen diffusion. The balance of evaporation and sticking (adsorption) is essential for the establishment of a local equilibrium vapor pressure at the dealloying front. As shown in Fig. 5, KMC simulations demonstrate that, in the limit of low sticking coefficient S_0, where atoms undergo multiple reflections before sticking, the dealloying kinetics is interface-controlled with the dealloying depth increasing linearly in time; in this limit VPD becomes directly analogous to electrochemical dealloying. In contrast, in the opposite limit without reflection (S_0=1), the dealloying kinetics is diffusion controlled with the dealloying depth increasing as $t^{1/2}$. KMC simulations further reveal that, in this S_0=1 limit, the dealloying rate is determined predominantly by surface diffusion, ballistic transport, or both, depending on the rate of evaporation relative to the rate of surface diffusion.

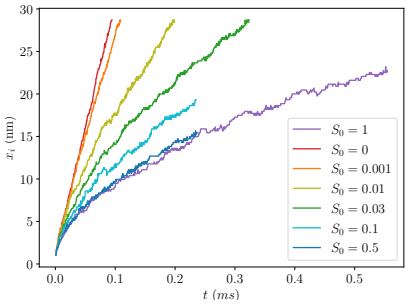

Fig. 5 KMC simulation of VPD showing a cross-over from interface- to diffusion controlled dealloying kinetics with increasing sticking coefficient.

Publications with DOE acknowledgement

1. "Phase-field crystal study of grain-boundary premelting", J. Mellenthin, A. Karma, and M. Plapp, *Phys. Rev.* B **78**, 184110 (2008).
2. "Method for computing short-range forces between solid-liquid interfaces driving grain boundary premelting", J. J. Hoyt, D. Olmsted, S. Jindal, M.Asta, and A. Karma, *Phys. Rev.* E **79**, 020601 (2009).
3. "Solidification microstructures and solid-state parallels: Recent developments, future directions", M. Asta, C. Beckermann, A. Karma, W. Kurz, R. Napolitano, M. Plapp, G. Purdy, M. Rappaz, and R. Trivedi, *Acta Materialia* **57**, 941–971 (2009).
4. "Laws of crack motion and phase-field models of fracture", V. Hakim and A. Karma, *J. Mech. Phys. Solids* **57**, 342-368 (2009).
5. "Phase-field crystal model for fcc ordering", K.-A. Wu, A. Adland, and A Karma, *Phys. Rev* E **81**, 061601 (2010).
6. "Multi-phase-field analysis of short-range forces between diffuse interfaces", N. Wang, R. Spatscheck, and A Karma, *Phys. Rev* E **81**, 051601 (2010).
7. "Amplitude equations for polycrystalline materials with interaction between composition and stress", R. Spatscheck and A Karma, *Phys. Rev* B **81**, 214201 (2010).
8. "Structural disjoining potential for grain-boundary premelting and grain coalescence from molecular-dynamics simulations", S. J. Fensin, D. Olmsted, D. Buta, M. Asta, A. Karma, and J. J. Hoyt, Phys. Rev. E **81**, 031601 (2010).
9. "Helical crack-front instability in mixed mode fracture", A. J. Pons and A. Karma, *Nature* **464**, 85-89 (2010).
10. "Phase-Field Modeling of Crack Propagation", R. Spatscheck, E. Brener, and A Karma, *Phil. Mag.* **91**, 75-95 (2011).
11. "Dislocation-Pairing Transitions in Hot Grain Boundaries", D. L. Olmsted, D. Buta, A. Adland, S. M. Foiles, M. Asta, and A. Karma, *Phys. Rev. Lett.* **106**, 046101 (2011).
12. "Theoretical analysis of crack front instability in mode I+III", J.-B. Leblond, A. Karma, and V. Lazarus, *J. Phys. Mech. Solids* **59**, 1872-1887 (2011).
13. "Surface modes of coherent spinodal decomposition", M. Tang and A. Karma, *Phys. Rev. Lett.* **108**, 265701 (2012).
14. "Coupled motion of asymmetrical tilt grain boundaries: Molecular dynamics and phase-field crystal simulations", Z.T. Trautt, A. Adland, A. Karma, and Y. Mishin, *Acta Materiala* **60**, 6528-6546 (2012).
15. "Relationship between Equilibrium Fluctuations and Shear-Coupled Motion of Grain Boundaries", A. Karma, Z.T. Trautt, and Y. Mishin, *Phys. Rev. Lett.* **109**, 095501 (2012).
16. "Structural short-range forces between solid-melt interfaces", R. Spatschek, A. Adland, and A. Karma, *Phys. Rev.* B**87**, 024109 (2013).
17. "Phase-field-crystal study of grain boundary premelting and shearing in bcc iron", A. Adland, A. Karma, R. Spatschek, D. Buta, and M. Asta, *Phys. Rev.* B**87**, 024110 (2013).

18. “Unified Theoretical Framework for Polycrystalline Pattern Evolution”, A. Adland, Y. Xu, and A. Karma, *Phys. Rev. Lett.* **110**, 265504 (2013).
19. “Phase-field modeling of grain-boundary premelting using obstacle potentials”, V. Sai Pavan Kumar Bhogireddy, C. Hüter, J. Neugebauer, I. Steinbach, A. Karma, and R. Spatschek, *Phys. Rev.* E**90**, 012401 (2014).
20. “Ginzburg-Landau theory of the bcc-liquid interface kinetic coefficient”, K.-A. Wu, C.-H. Wang, J.J. Hoyt, and A. Karma*, Phys. Rev.* B **91**, 014107 (2015).
21. “Morphological instability of grain boundaries in two-phase coherent solids”, P.-A. Geslin, Y. Xu, and A. Karma, *Phys. Rev. Lett.* **114**, 105501 (2015).
22. “Multiscale cohesive zone model for propagation of segmented crack fronts in mode I+III fracture”, J.-B. Leblond, V. Lazarus, and A. Karma, *Int. J. Fracture* **191**, 167-189 (2015).
23. “Three-Dimensional Multiscale Modeling of Dendritic Spacing Selection During Al-Si Directional Solidification”, D. Tourret, A.J. Clarke, S.D. Imhoff, P.J. Gibbs, J.W. Gibbs, and A. Karma, *JOM* **67**, 1776-1785 (2015).
24. “Three-dimensional Dendritic Needle Network model with application to Al-Cu directional solidification experiments”, D. Tourret, A. Karma, A.J. Clarke, P.J. Gibbs, S.D. Imhoff, IOP Conf. Series: Materials Science and Engineering **84**, 012082 (2015).
25. “Crack Front Segmentation and Facet Coarsening in Mixed-Mode Fracture”, C.-H. Chen, T. Cambonie, V. Lazarus, M. Nicoli, A.J. Pons, and A. Karma, *Phys. Rev. Lett.* **115**, 265503 (2015).
26. “Topology-generating interfacial pattern formation during liquid metal dealloying”, P.-A. Geslin, I. McCue, J. Erlebacher, and A. Karma, *Nature Communications* **6**, 8887 (2015).
27. “Atomistic to continuum modeling of solidification microstructures”, A. Karma and D. Tourret, *Current Opinion in Solid State and Materials Science* **20**, 25-36 (2016).
28. “Two-mode Ginzburg-Landau theory of crystalline anisotropy for fcc-liquid interfaces”, K.-A. Wu, S.-C. Lin, and A. Karma, *Phys. Rev.* B **93**, 054114 (2016).
29. “Kinetics and morphological evolution of liquid metal dealloying”, I. McCue, B. Gaskey, P.A. Geslin, A. Karma, and J. Erlebacher, *Acta Materialia* **115**, 10-23 (2016).
30. “Elastically mediated interactions between grain boundaries and precipitates in two-phase coherent solids”, Y.-C. Xu, P.-A. Geslin, and A. Karma, *Phys. Rev.* B **94**, 144106 (2016).
31. “Grain growth competition during thin-sample directional solidification of dendritic microstructures: A phase-field study”, D. Tourret, Y. Song, A. J. Clarke, and A. Karma*, Acta Materialia* **122**, 220-235 (2017).
32. “Instability in dynamic fracture and the failure of the classical theory of cracks”, C-H. Chen, E. Bouchbinder, and A. Karma, *Nature Physics* **13**, 1186 (2017).
33. “Pattern formation during electrochemical and liquid metal dealloying”, I. McCue, A. Karma, and J. Erlebacher, *MRS Bull*. **43**, 27-34 (2018).
34. “Universality and Stability Phase Diagram of Two-Dimensional Brittle Fracture”, Y. Lubomirsky, C-H. Chen, A. Karma, and E. Bouchbinder, *Phys. Rev. Lett.* **121,** 134301 (2018).
35. “Configurational stability of a crack propagating in a material with mode-dependent fracture energy - Part I: Mixed-mode I + III”, J.B. Leblond, A. Karma, L. Ponson, A. Vasudevan, *J. Mech. Phys. Solids* **126**, 187–203 (2019).

36. "Phase-field modeling of chemomechanical fracture of intercalation electrodes: Role of charging rate and dimensionality", A. Mesgarnejad and A. Karma, *J. Mech. Phys. Solids* **132**, 103696 (2019).
37. "Influence of morphological instability on grain boundary trajectory during directional solidification", S. Ghosh, A. Karma, M. Plapp, S. Akamatsu, S. Bottin-Rousseau, G. Faivre, *Acta Mater.* **175**, 214-221 (2019).
38. "Configurational stability of a crack propagating in a material with mode-dependent fracture energy - Part II: Drift of fracture facets in mixed-mode I+II+III", A. Vasudevan, L. Ponson, A. Karma, J.B. Leblond, *J. Mech. Phys. Solids* **137**, 103894 (2020).
39. "Vulnerable window of yield strength for swelling-driven fracture of phase-transforming battery materials", A. Mesgarnejad and A. Karma, *npj Computational Materials* **6**, 58 (2020).
40. "Vapor phase dealloying kinetics of MnZn alloys", Lu, Z., Zhang, F., Wei, D., Han, J., Xia, Y., Jiang, J., Zhong, M., Hirata, A., Watanabe, K., Karma, A. and Erlebacher, J., Chen, M. *Acta Materialia* **212**, 116916 (2021).
41. "Fragmentation of faceted crystalline wires.", N. Wang and A. Karma. *Physical Review Mat.* **6**: 106002 (2022).
42. L. Lai, B. Gaskey, A. Chuang, J. Erlebacher, and A. Karma. "Topological control of liquid-metal-dealloyed structures." *Nature communications* **13**, 1-10 (2022).
43. "Microstructural pattern formation during liquid metal dealloying: Phase-field simulations and theoretical analyses", L. Lai, P.-A. Geslin, and A. Karma, *Physical Review Mat.* **6**: 093803 (2022).
44. "Topology-enhanced mechanical stability of swelling nanoporous electrodes", B. E. Grossman-Ponemon, A. Mesgarnejad, and A. Karma, submitted to *npj Computational Materials* (2022).
45. "Bicontinuous structure formation by peritectic melting", M. Zhong, L. Lai, and A. Karma, *in preparation*.
46. "Kinetic Monte Carlo Study of Vapor Phase Dealloying", L. Lai and A. Karma, *in preparation.*